International Journal of Bio-resource and Stress Management https://ojs.pphouse.org/index.php/IJBSM

Crossref

IJBSM October 2025, 16(10): 01-08 **Article** AR6447

Research Article *Stress Management*

DOI: HTTPS://DOI.ORG/10.23910/1.2025.6447

Comprehensive Diagnostic Anatomy of Normal and Osteoarthritic Canine Stifle Joint

N. Gupta[1], R. Vaish[1], A. Shahi[2], D. K. Gupta[3], A. Mishra[2], P. Jain[1], A. Dubey[4] and S. Tekam[1]

[1]Dept. of Veterinary Anatomy, [2]Dept. of Veterinary Surgery and Radiology, [3]Dept. of Veterinary Medicine, [4]Dept. of Veterinary Pathology, College of Veterinary Science and A. H., Nanaji Deshmukh Veterinary Science University, Jabalpur, Madhya Pradesh (482 001), India

Open Access

Corresponding dr.nidhivety@yahoo.co.in

0009-0006-8043-5144

ABSTRACT

The experiment was conducted from October, 2021 to August, 2023 at the Veterinary College, Jabalpur, to study the stifle joint of dogs, to investigate morphological alterations in osteoarthritic stifle joints using radiography, computed tomography (CT), and ultrasonography, and to compare them with those of healthy stifle joints. In addition to these, gross observations of the stifle joint are recorded in the carcasses of dogs to set baseline data. Osteoarthritis is a disease characterized by an imbalance between the synthesis and degeneration of articular cartilage components. The stifle joint is a complex synovial joint prone to osteoarthritis. Present work was conducted on the stifle joint of 24 dogs, divided into three groups: group I and II, which included carcasses of 06 young (3-5 months) and 06 adult (more than one year) indigenous non- lame dogs, respectively, as control and group III comprised of 12 clinical cases of stifle osteoarthritis. In group II, the cranial cruciate ligament consisted of distinct craniomedial and caudolateral bundles, whereas in group I, no clear separation was seen grossly. Radiographic and CT observations showed the presence of a growth plate as a radiolucent gap between the epiphysis and metaphysis in group I dogs, while increased subchondral bone opacity at the tibial epiphysis, with osteophytes and uneven condylar margins, was visible in group III. The results of this study will be useful in the customized treatment of stifle osteoarthritis.

KEYWORDS: Computed tomography, dog, diagnostic anatomy, osteoarthritis, stifle joint

***Citation* (VANCOUVER):** Gupta et al., Comprehensive Diagnostic Anatomy of Normal and Osteoarthritic Canine Stifle Joint. *International Journal of Bio-resource and Stress Management,* 2025; 16(10), 01-08. HTTPS://DOI.ORG/10.23910/1.2025.6447.

Data Availability Statement: Legal restrictions are imposed on the public sharing of raw data. However, authors have full right to transfer or share the data in raw form upon request subject to either meeting the conditions of the original consents and the original research study. Further, access of data needs to meet whether the user complies with the ethical and legal obligations as data controllers to allow for secondary use of the data outside of the original study.

Conflict of interests: The authors have declared that no conflict of interest exists.

RECEIVED on 16th June 2025 RECEIVED in revised form on 02nd October 2025 ACCEPTED in final form on 18th October 2025 PUBLISHED on 31st October 2025

1. INTRODUCTION

Dogs provide the best company for humans and have done so for many years. Dog joints need to be free of disease and in good condition for them to move around. The stifle joint is a complex, condylar, synovial joint that allows motion in three planes. The complexity of the normal motion is directly related to the structure and functions of the anatomical components that form the joint (Carpenter Jr and Cooper, 2000; Al-Juhaishi and Khalil, 2023). Movements of this joint are a function of the complex integration of the condylar portion of the distal femur, proximal tibia, and proximal fibula, as well as the pelvic limb muscles, joint capsule, joint ligaments, and menisci (Robins, 1990). Four sesamoid bones are present in the vicinity of the stifle joint: the patella, the medial and lateral fabella, and the popliteal sesamoid bone (Ballegeer, 2016). This joint is prone to osteoarthritis occurring as a result of structural instabilities like rupture of the cranial cruciate ligament (Kobayashi et al., 2006; Hayashi et al., 2003), malalignment after fracture, or abnormal load distribution on the cartilage. Partial tearing of the ligament is common and frequently progresses to a full tear over time, especially when left untreated. When this condition develops with one knee, there is an increased chance of similar problem in other knee sometime in the future. Understanding the normal anatomy of the stifle joint, particularly cruciate ligaments anatomy, is essential for diagnosis and rational treatment of cranial cruciate ligament rupture (Sherman, 2007). Because of their anatomy and spatial arrangement, the cruciate ligaments provide primary ligamentous support for craniocaudal and axial stability of the stifle joint throughout the functional range of motion. As stifle osteoarthritis is a chronic and progressive disease, it leads to severe pain and significant restrictions on movement. There is also the emotional cost to the owner dealing with an animal that is chronically or terminally unwell and/or in chronic pain, which can cause psychological distress and upset. Stifle joint is suspected for any affection or injury when an animal exhibits lameness, signs of pain and/or swelling of the joint. Different imaging techniques are used to investigate the source of pathology, and among all modalities, radiography is one of the most common methods used for the diagnosis of joint or skeletal abnormalities. Radiographic signs of osteoarthritis include joint effusion, osteophytosis (Felson et al., 2005), enthesophytes formation, soft tissue swelling, sclerosis in the subchondral region and mineralization in the intra-articular region (Innes, 2018; Yamazaki et al., 2021; Roitner et al., 2024). Although many methods are used for radiological assessment of arthritis, it is still necessary to grade images of stifle osteoarthritis to quantify the severity and compare changes (Kohn et al., 2016; Rhee et al., 2023). Radiography of joints is the simplest and easiest way for the detection of osteoarthritis but computed tomography offers thorough details on every component that a standard radiography examination may overlook (Jones et al., 2022; Chung et al., 2023). As our understanding of the structural and functional components increases, accurate detection and successful characterization of early osteoarthritic events becomes possible by that better and lasting treatment options may be explored. Thus, the present work was planned to assess clinical and radiographic changes of stifle osteoarthritis and the simultaneous evaluation of a normal joint to set baseline morphological data for comparison.

2. MATERIALS AND METHODS

The experiment was conducted from October, 2021 to August, 2023 at the Veterinary College, Jabalpur, to study the stifle joint of dogs. 24 dogs, divided into three groups; in group I and II, there were carcasses of 06 young (3-5 months) and 06 adult (more than one year) indigenous non-lame dogs, respectively, as control and group III comprised 12 clinical cases of stifle osteoarthritis. Carcasses of indigenous dogs were procured from the Veterinary Clinical Complex, Jabalpur, that died or were euthanized for reasons unrelated to diseases of the stifle joint. Selection of dogs of group III was done by screening of 120 dogs showing lameness in the hind limb, irrespective of age, breed and sex, brought to Veterinary Clinical Complex, Jabalpur. Screening was carried out on the basis of history, clinical examination and radiography. The duration of the study was two years, i.e., from October, 2021 to August, 2023. The study was approved by the institutional animal ethical committee of NDVSU, Jabalpur (53/IAEC/Vety/2021, dated 26.10.2021) and complies with CPCSEA guidelines (registration number 2071/GO/Re/S/19/CPCSEA).

2.1. Clinical examination

Clinical lameness scoring for assessment of osteoarthritis in dogs was carried out using an ordinal scoring system (McCarthy et al., 2007) mentioned in Table 1.

2.2. Gross examination

To observe the normal anatomy of the stifle joint, dissection was performed on carcasses. After dissection, examination and measurement (cm) of articular structures and ligaments were made and differences between group I and II were noted.

2.3. Radiographic examination

Standard Antero-posterior and medio-lateral radiographic views of the stifle were taken with an X-ray unit (Ultimax-50) assembled with the CR system (Carestream). The X-ray machine was set on 8mAs, while kilovoltage was determined following Sante's rule (2×thickness+40), according to the dog's size and age. Based on radiographic images, stifle

Table 1: Clinical lameness scoring system for assessing dogs with osteoarthritis

Criterion	Clinical evaluation
Lameness	1. Walks normally
	2. Slightly lame when walking
	3. Moderately lame when walking
	4. Severely lame when walking
	5. Reluctant to rise and will not walk more than five paces
Joint mobility	1. Full range of motion
	2. Mild limitation (10–20%) in range of motion; no crepitus
	3. Mild limitation (10–20%) in range of motion; with crepitus
	4. Moderate limitation (20–50%) in range of motion; ±crepitus
	5. Severe limitation (>50%) in range of motion; ±crepitus
Pain on palpation	1. None
	2. Mild signs; dog turns head in recognition
	3. Moderate signs; dog pulls limb away
	4. Severe signs; dog vocalises or becomes aggressive
	5. Dog will not allow palpation
Weight-bearing	1. Equal on all limbs standing and walking
	2. Normal standing; favors affected limb when walking
	3. Partial weight-bearing standing and walking
	4. Partial weight-bearing standing; non-weight-bearing walking
	5. Non-weight-bearing standing and walking
Overall score of clinical condition	1. Not affected
	2. Mildly affected
	3. Moderately affected
	4. Severely affected
	5. Very severely affected

osteoarthritis was graded according to the Kellgren and Lawrence (1957) radiographic score mentioned in Table 2.

2.4. Computed tomography

A computed tomography (CT) scan of the stifle joint was performed in dorsal recumbency with flexed stifle joint flexed. The dogs were given atropine @ 0.02 mg kg^{-1} body weight, intramuscular, followed by inj. xylazine @ 1 mg kg^{-1} and inj. ketamine HCl @ 5 mg kg^{-1} intramuscular. 5mm-thick contiguous CT slices were generated, having a reconstruction index of 0.5mm, using Fujifilm, Supria 16ch/32 slice CT. The original CT data were transferred as DICOM images to an image analysis workstation to perform the image analysis. The original transverse slices were reformatted into the sagittal and dorsal planes. The window was also adjusted as required to better define bone margins. The opacity of all structures was observed, and articular margins were evaluated for irregularities, including sclerosis, osteophytes, altered morphology and bone density (Hounsfield unit) for the affected stifle joint.

2.5. Statistical analysis

Statistical analysis was done with the help of R software (R team 2013) using an independent t-test and applied descriptive statistics (p<0.05).

3. RESULTS AND DISCUSSION

3.1. Clinical assessment and occurrence of stifle osteoarthritis

A total of 120 dogs with hind limb lameness were screened on the basis of history. Clinical examination and further radiography (Bland, 2015; McCarthy et al., 2007) revealed 12 dogs affected with unilateral stifle osteoarthritis. The score of the clinical assessment is depicted in Table 3.

3.2. Gross examination

The joint capsule of the stifle joint was extensive and

Table 2: Grading of stifle osteoarthritis based on radiographic score

Grade	Classification	Description
1.	Slight	Slightly detectable small osteophytes and/or roughness, no sclerosis, no bone deformity
2.	Mild	Definite, small to moderate osteophytes, possible sclerosis, no bone deformity
3.	Moderate	Multiple and moderate to large osteophytes, initiating sclerosis, possibly initiating bone deformity
4.	Severe	Multiple and large osteophytes, sclerosis, and advanced bone deformity

capacious; it forms three sacs: the patellar sac, the lateral and medial femoro-tibial sacs, all of which freely intercommunicate. Just below the patella synovial and fibrous layers of the joint capsule are separated by a fat pad. The four femorotibial ligaments were observed, i.e., medial and lateral collateral ligaments; cranial and caudal cruciate ligaments. The medial collateral ligament had wide attachments at its origin and insertion and a narrow middle portion, adopting an hourglass shape. It originated in the distal femur and inserted on the proximal tibia, and was also intimately attached to the medial meniscus. The lateral collateral ligament extends from the lateral epicondyle of the femur to the head of the fibula (with a few fibers attaching to the lateral condyle of the tibia). The lateral collateral ligament had a course over the tendon of origin of the popliteus muscle. The lateral collateral ligament did not show any distinct attachments to the lateral meniscus. The hourglass appearance and meniscal attachments of the medial collateral ligament are in accordance with the study of Palierne et al. (2022). The firm attachment of the medial collateral ligament to the medial meniscus is the reason for its less mobility compared to the lateral meniscus (Arnoczky, 1993; Abumandour et al., 2020). This arrangement facilitates more movement of the lateral femoral condyle, which helps in the basic motion associated with the screw home mechanism. Both collateral ligaments contribute to the minimization of varus and valgus angulation of the tibia during extension. However, during flexion, as there is loosening of the lateral collateral ligament to some extent, there can be limited varus and valgus angulation. The collateral ligaments work in coordination with the cruciate ligaments to provide rotational stability to this joint.

Table 3: Clinical scoring of stifle osteoarthritis

No. of dogs	Score				
	Lame-ness	Joint mobility	Pain on palpation	Weight-bearing	Overall score of clinical condition
6	3	3	4	4	3
6	3	2	2	3	2

The cranial cruciate ligament (CrCL) has a fan-shaped origin from the caudomedial part of the lateral femoral condyle; it then narrows down, spirals, and runs cranially, medially, and distally to insert again in a fan-like fashion over the cranial intercondylar area of the tibia. The caudal cruciate ligament (CCL) courses from the lateral side of the medial femoral condyle, runs caudally and distally, crossing the CrCL medially. Finally, it was inserted on the medial aspect of the popliteal notch of the tibia. Craniomedial and caudolateral bundles of CrCL were observed in group II. However, in group I, separate bundles of the cranial cruciate ligament were not distinct (Figure 1). Both ligaments were narrowest in their middle and fan out at either end; the core in the middle region has fewer blood vessels. Attachments of cruciate ligaments at tibial and femoral ends described in the present study are in agreement with the findings of Rooster et al. (2006), who found slightly more width of the caudal cruciate ligament than the cranial cruciate ligament, in opposition to the present observation. Being the narrowest and having the least blood supply in the middle region (Kobayashi et al., 2006), any minor injury and pressure to the cruciate ligaments further reduces blood supply, leading to slow healing and repair, which further causes weakening of the ligaments (Arnoczky et al., 1979; Vasseur et al., 1985).

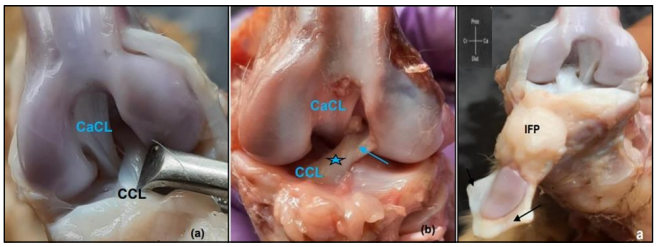

Figure 1: Photograph of stifle joint (a) group I (b) group II: showing cranial (CCL) and caudal cruciate ligament (CaCL); craniomedial (asterisk) and caudolateral (↑ blue) bundles of CCL; infrapatellar fat pad (IFP) and medial & lateral femoropatellar ligaments (↑)

There was a single broad patellar ligament connecting the patella to the tibial tuberosity. It was separated from the joint capsule by the infrapatellar fat pad. Towards the tibial end, this fat pad was thick compared to the femoral end (Figure 1). The Sides of the patella were connected to the femur by the medial and lateral femoropatellar ligaments. They were partially blended with the overlying femoral fasciae (Figure 1). These findings corroborate the observations of Evans and Lahunta (2013). The mean values of measurements of

stifle joint ligaments were significantly higher in the dogs of group II as compared to group I; results of the same are depicted in Table 4.

Table 4: Length (cm) and width (cm) of stifle joint ligaments

	Parameter	Group I	Group II
	Length of the medial collateral ligament	2.35^{b}±0.02	4.07^{a}±0.04
	Length of the lateral collateral ligament	2.06^{b}±0.03	3.75^{a}±0.03
Patellar ligament			
	Length	3.73^{b}±0.04	6.5^{a}±0.04
Width	At the femoral end	0.76^{b}±0.02	1.78^{a}±0.02
	At middle	0.97^{b}±0.03	1.17^{a}±0.02
	At the tibial end	0.65^{b}±0.02	1.07^{a}±0.02
Cranial cruciate ligament			
	Length	1.00^{b}±0.04	1.49^{a}±0.02
	Width at the middle	0.48^{b}±0.03	0.53^{a}±0.02
Caudal cruciate ligament			
	Length	1.17^{b}±0.03	1.61^{a}±0.02
	Width at the middle	0.38^{b}±0.03	0.53^{a}±0.02

Mean values between the groups (a, b) with different superscripts varied significantly (p<0.05)

3.3. *Radiographic observations*

Measurement of joint space and thickness of epiphysis was recorded in the mediolateral view of radiographs. Joint space was significantly wider in group I compared to group II (Table 5). Beneath the articular cartilage, there was a subchondral bone plate, which was a radio-opaque plate of uniform thickness. Perichondral bone opacity was not evident in any of the radiographs of groups I and II (Figure 2). Radiolucent gap between epiphysis and metaphysis represented the presence of a growth plate, as well as a separate ossification centre for tibial tuberosity was observed in group I (Figure 2). Before the final interpretation of radiographs of group III (osteoarthritis), interobserver variances were also clarified (Wessely et al., 2017). The mediolateral radiograph of the stifle joint in one clinical case showed increased subchondral bone opacity at the tibial epiphysis and increased synovial mass (Gilbert et al., 2019). Enthesophyte formation above the patella was observed (Figure 3). In the stifle, the infrapatellar fat pad sign (Allan and Davies, 2018) was used to evaluate synovial mass in osteoarthritis cases of the present study. The normal infrapatellar fat pad is recognized easily on medio-lateral stifle radiographs as a relatively radiolucent triangular space between the cranial tibial plateau, the distal condyles of the

Table 5: Radiographic measurements (cm) of the stifle joint

Parameter	Group I	Group II
Joint space		
Middle	0.43^{a}±0.01	0.23^{b}±0.02
Thickness of the distal femoral epiphysis		
Cranial	0.80^{b}±0.10	1.07^{a}±0.02
Middle	1.47±0.06	1.39±0.04
Caudal	1.24±0.03	1.27±0.02
Thickness of the proximal tibial epiphysis		
Cranial	0.65^{b}±0.01	0.93^{a}±0.05
Middle	0.51^{b}±0.01	1.02^{a}±0.01
Caudal	0.34^{b}±0.01	0.79^{a}±0.02

Mean values between the groups (a, b) with different superscripts varied significantly (p<0.05)

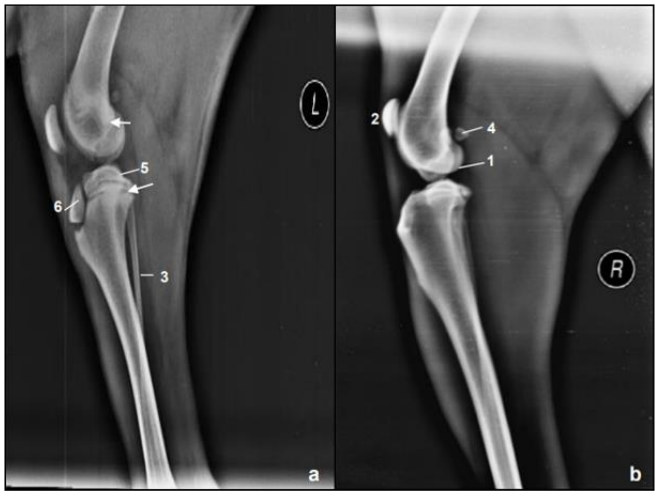

Figure 2: Mediolateral radiograph of stifle joint (a) group I, (b) group II, showing 1. condyle of femur; 2. patella; 3. fibula; 4. fabella bone; 5. tibial condyle; 6. ossification centre (OC) of tibial tuberosity, physis (arrow)

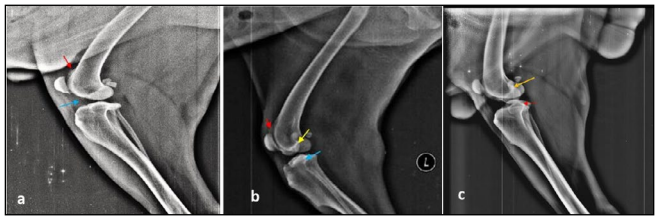

Figure 3: Mediolateral radiograph of stifle joint: a: Showing increased subchondral bone opacity, enthesophyte above patella (↑), increased synovial mass, represented by altered shape of the fat pad (↑) in a 4-year Labrador; b: showing increased subchondral bone opacity (↑), spur formation at the condyle of the femur (↑), enthesophyte above the patella (↑) in a 5-year-old Labrador; c: showing osteophyte near the fabella bone (↑) and proximal tibia (↑) in an 8-year-old Labrador

femur, and the patellar ligament's insertion on the cranial tibial tuberosity. When the stifle synovial mass increased (may be due to increased synovial fluid or changes in soft tissue), the shape of the fat pad altered and became a radio-dense "gray cloud". Increased subchondral bone opacity is the response to articular cartilage thinning (Intema et al., 2010). In another clinical case, a mediolateral radiograph showed enthesophyte formation above the patella and radio-opaque structure above condyles identifiable as osteophytes formation (Felson et al., 2005), a triangular area behind the patellar ligament, and between stifle and tibia showed no change of altered synovial fluid volume or synovial mass (Figure 3). Risk factors for stifle joint osteoarthritis included ruptured cranial cruciate ligaments, patellar luxation and obesity (Ramírez-Flores et al., 2017; Alves et al., 2020; Villatoro et al., 2020). Radiographic score of stifle osteoarthritis according to Kellgren and Lawrence (1957) was calculated and found 50% dogs with grade 3 osteoarthritis and the remaining 50% suffered from grade 2.

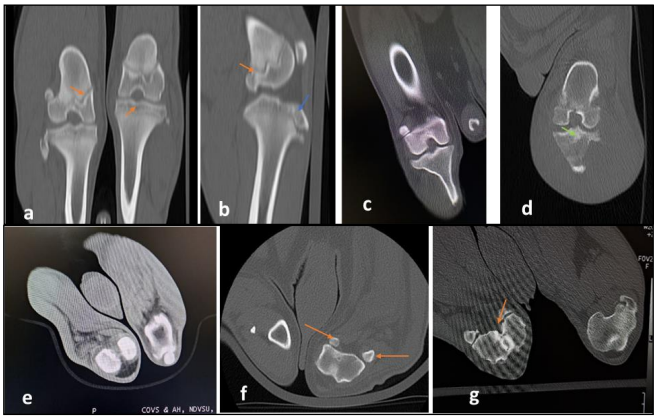

Figure 4: Computed Tomography scan images of the stifle joint: a and b: Sagittal reconstruction (group I), arrows show physis, blue arrow shows ossification centre of the tibial tuberosity; c: Dorsal reconstruction (group II) showing even margins of femoral and tibial condyles; d: dorsal reconstruction (group III) showing uneven margins of femoral and tibial condyles and osteophytes at the proximal tibia (arrow); e and f: Transverse reconstruction of the distal femur (group II) showing a normal anatomical picture, arrow showing the fabellae bones; g: bridging of the intercondylar space due to sclerosis and osteophyte formation (group III)

3.4. Computed tomographic observations

In normal stifle CT scans of group I and II, there was good demarcation between medulla and cortex when Images were made using the bone window. The physis (growth plate) was well depicted in group I and the articular cartilage was seen as a hyperdense line (Figures 4a and b). The visibility and density of the menisci, tibial and femoral condyles, and other structures of the stifle in group II (Figure 4c, e and f) on CT in this study were similar to previous reports (Soler et al., 2007; Gielen and Bree, 2017).

In dogs of group III (Stifle osteoarthritis), identification and quantitative assessment of the presence of even a single osteophyte was done. Assessment of the degree of subchondral bone changes was made and found that subchondral bone opacity was increased in the osteoarthritic stifle joint. Moreover, there was a decrease in joint space and sclerosis of bony margins (Figure 4d and g). There were changes in Hounsfield unit (HU) around the margins of the epiphysis and subchondral region in the osteoarthritic stifle joint in comparison to the normal joint. Osteophytes showed radiodensity between 410-915 HU, depending upon extent of calcification. Subchondral bone was more radiodense with 1350-1450 HU due to sclerosis, in comparison to radiodensity of normal femoral and tibial condyles (900-1000 HU). Additional clinical applications in veterinary diagnostics are made possible by the versatility of CT exams for image capture and reconstruction (Bertolini et al., 2003).

4. CONCLUSION

An accurate description of the complex ligament in detail would be helpful in unravelling the etiopathogenesis of stifle osteoarthritis. A thorough understanding of normal stifle anatomy would be an asset for the correct assessment and definition of injury. The observations of the above study served as a baseline reference for the interpretation of radiography and CT scans of stifle joint in dogs and might be helpful to clinicians in the assessment of its pathological conditions and development of customized treatment.

5. FURTHER RESEARCH

Assessment of osteoarthritic stifle joint using magnetic resonance imaging technique for a precise understanding of the cause and treatment of this disease.

6. ACKNOWLEDGEMENT

We are appreciative of the cooperation from pet owners in carrying out this research. The authors wish to sincerely thank those who donated their pet bodies to science so that anatomical research could be performed.

7. REFERENCES

Abumandour, M.M.A., Bassuoni, N.F., El-Gendy, S., Karkoura, A., El-Bakary, R., 2020. Gross-anatomical, radiographic and computed tomographic study of the stifle joint of donkeys (Equus africanus asinus). Anatomia Histologia Embryologia 49, 402–416. https://doi.org/10.1111/ahe.12543.

Al-Juhaishi, O., Khalil, N., 2023. Anatomical study of stifle joint in dogs. Tikrit Journal of Veterinary Sciences 23, 68–78. 10.25130/tjvs.23.1.7.

Allan, G., Davies, S., 2018. Radiographic signs of joint disease in dogs and cats. In: Thrall, D.E. (Ed.). Textbook of veterinary diagnostic radiology, seventh ed., W.B. Saunders, 403–433.

Alves, J.C., Santos, A., Jorge, P., Lavrador, C., Carreira, L.M., 2020. Clinical and diagnostic imaging findings in police working dogs referred for hip osteoarthritis. BMC Veterinary Research 16, 425. https://doi.org/10.1186/s12917-020-02647-2.

Arnoczky, S.P., 1993. Pathomechanics of cruciate ligament and meniscal injuries. In: Bojrab, M.J. (Ed.), Disease mechanisms in small animal surgery, Philadelphia: Lea & Febiger, 764–776.

Arnoczky, S.P., Rubin, R.M., Marshall, J.L., 1979. Microvasculature of the cruciate ligaments and its response to injury. Journal of Bone and Joint Surgery 61A, 1221–1229. https://pubmed.ncbi.nlm.nih.gov/511882/.

Ballegeer, E.A., 2016. Computed tomography of the musculoskeletal system. Veterinary Clinics of North America: Small Animal Practice 46(3), 373–420, https://doi.org/10.1016/j.cvsm.2015.12.005.

Bertolini, G., Furlanello, T., Caldin, M., 2003. Preliminary experiences and clinical applications of multislice-CT in small animal practice. In: Proceedings of the Autumn Meeting, European Association of Veterinary Diagnostic Imaging, Cambridge, UK, 29.

Bland, S.D., 2015. Canine osteoarthritis and treatments: a review. Veterinary Science Development 5(2). https://doi.org/10.4081/vsd.2015.593.1.

Carpenter Jr, D.H., Cooper, R.C., 2000. Mini review of canine stifle joint anatomy. Anatomia Histologia Embryologia 29(6), 321–329. doi: 10.1046/j.1439-0264.2000.00289.x. PMID: 11199475.

Chung, C.S., Tu, Y.J., Lin, L.S., 2023. Comparison of digital radiography, computed tomography, and magnetic resonance imaging features in canine spontaneous degenerative stifle joint osteoarthritis. Animals 13(5), 849. https://doi.org/10.3390/ani13050849.

Evans, H.E., De Lahunta, A., 2013. Miller's anatomy of the dog, 4th Ed., St. Louis, Saunders/Elsevier, pp. 268–280. PMCID: PMC4790228.

Felson, D.T., Gale, D.R., Elon, Gale, M., Niu, J., Hunter, D.J., Goggins, J., Lavalley, M.P., 2005. Osteophytes and progression of knee osteoarthritis. Rheumatology 44(1), 100–104. https://doi.org/10.1093/rheumatology/keh411.

Gielen, I., Bree, H.V., 2017. Computed tomography of the stifle. In: Muir, P. (Ed), Advances in the canine cranial cruciate ligament (2nd Edn). Wiley Blackwell, 141–154. https://doi.org/10.1002/9781119261728.ch20.

Gilbert, S., Langenbach, A., Marcellin-Little, D.J., Pease, A.P., Ru, H., 2019. Stifle joint osteoarthritis at the time of diagnosis of cranial cruciate ligament injury is higher in Boxers and in dogs weighing more than 35 kilograms. Veterinary Radiology and Ultrasound 60(3), 280–288. https://doi.org/10.1111/vru.12718.

Hayashi, K., Frank, J.D., Dubinsky, C., Zhengling, H., Markel, M.D., Manley, P.A., Muir, P., 2003. Histologic changes in ruptured canine cranial cruciate ligament. Veterinary Surgery 32(3), 269–77. doi: 10.1053/jvet.2003.50023. PMID: 12784204.

Innes, J.F., Costello, M., Barr, F.J., Rudorf, H., Barr, A.R.S., 2004. Radiographic progression of osteoarthritis of the canine stifle joint: a prospective study. Veterinary Radiology and Ultrasound 45(2), 143–148.

Intema, F., Hazewinkel, H.A.W., Gouwens, D., Bijlsma, J.W.J., Weinans, H., Lafeber, F.P.J.G., Mastbergen, S.C., 2010. In early OA, thinning of the subchondral plate is directly related to cartilage damage: results from a canine ACLT-meniscectomy model. Osteoarthritis and Cartilage 18(5), 691–698. https://doi.org/10.1016/j.joca.2010.01.004.

Jones, G.M.C., Pitsillides, A.A., Meeson, R.L., 2022. Moving beyond the limits of detection: the past, the present, and the future of diagnostic imaging in canine osteoarthritis. Frontiers in Veterinary Science 15(9), 789898. DOI: 10.3389/fvets.2022.789898.

Kellgren, J.H., Lawrence, J.S., 1957. Radiological assessment of osteo-arthrosis. Annals of Rheumatic Diseases 16, 494–502. https://doi.org/10.1136/ard.16.4.494.

Kobayashi, S., Baba, H., Uchida, K., Negoro, K., Sato, M., Miyazaki, T., Nomura, E., Murakami, K., Shimizubata, M., Meir, A., 2006. Microvascular system of anterior cruciate ligament in dogs. Journal of Orthopedic Research 24(7), 1509–1520. doi: 10.1002/jor.20183. PMID: 16732615.

Kohn, M.D., Sassoon, A.A., Fernando, N.D., 2016. Classifications in brief: Kellgren Lawrence classification of osteoarthritis. Clinical Orthopedic and Related Research 474, 1886–1893.

McCarthy, G., O'Donovan, J., Jones, B., McAllister, H., Seed, M., Mooney, C., 2007. Randomised double-blind, trial to assess the efficacy of glucosamine/chondroitin sulfate for the treatment of dogs with osteoarthritis. Veterinary Journal 174(1), 54–61. https://doi.org/10.1016/j.tvjl.2006.02.015.

Palierne, S., Blondel, M., André Autefage, K.V., 2022. Morphometric assessment of the medial collateral ligament of the canine stifle joint. Research in Veterinary Science 151, 21–26. https://doi.org/10.1016/j.rvsc.2022.06.032.

R Core Team, 2013. R: A language and environment for statistical computing. R Foundation for Statistical Computing, Vienna.

Ramírez-Flores, G.I., Del Angel-Caraza, J., Quijano-Hernández, I.A., Hulse, D.A., Beale, B.S., Victoria-Mora, J.M., 2017. Correlation between osteoarthritic changes in the stifle joint in dogs and the results of orthopaedic, radiographic, ultrasonographic and arthroscopic examinations. Veterinary Research Communication 41(2), 129–137. http://www.R-project.org/.

Rhee, B., Jin, C., Shin, S.H., Choi, H., Lee, Y., Kim, S., 2023. Establishment of an image evaluation grading criteria for experimental stifle joint osteoarthritis in dogs: an X-ray and CT imaging study. Laboratory animal research 39(1), 34. https://doi.org/10.1186/s42826-023-00186-z.

Robins, G.M., Whittick, W.G., 1990. Canine orthopedics. Lea and Febiger, Philadelphia, 693–702.

Roitner, M., Klever, J., Reese, S., Lindenberg, A.M., 2024. Prevalence of osteoarthritis in the shoulder, elbow, hip and stifle joints of dogs older than 8 years. The Veterinary Journal 305, 106132. https://doi.org/10.1016/j.tvjl.2024.106132.

Rooster, H., Bruin, T., Bree, P., 2006. Morphologic and functional features of the canine cruciate ligaments. Veterinary Surgery 35, 769–780. https://doi.org/10.1111/j.1532-950x.2006.00221.x.

Sherman, O.C., 2007. The canine stifle. Clinical Techniques in Small Animal Practice 22(4), 195–205, ISSN 1096-2867. https://doi.org/10.1053/j.ctsap.2007.09.008.

Soler, M., Murciano, J., Latorre, R., Belda, E., Rodrıguez, M.J., Agut, A., 2007. Ultrasonographic, computed tomographic and magnetic resonance imaging anatomy of the normal canine stifle joint. The Veterinary Journal 174, 351–361.

Vasseur, P.B., Pool, R.R., Arnoczky, S.P., Lau, R.E., 1985. Correlative biomechanical and histological study of the cranial cruciate ligament in dogs. American Journal of Veterinary Research 45, 1842–1854.

Villatoro, A., Langenbach, A., Yoon, J., Garcia, T., Marcellin-Little, D., 2022. Stifle joint osteoarthritis in small-breed and medium-breed dogs is more severe after cranial cruciate ligament injury than medial patellar luxation. Veterinary Radiology and Ultrasound. 64. 10.1111/vru.13207.

Wessely, M., Bruhschwein, A., Schnabl-Feichter, E., 2017. Evaluation of intra-and inter-observer measurement variability of a radiographic stifle osteoarthritis scoring system in dogs. Veterinary and Comparative Orthopaedics and Traumatology 30(06), 377–384.

Yamazaki, A., Edamura, K., Tomo, Y., Seki, M., Asano, K., 2021. Variations in gene expression levels with severity of synovitis in dogs with naturally occurring stifle osteoarthritis. PLoS ONE 16(1), 1–10.